Received: 18 March 2020 | Revised: 2 May 2020 | Accepted: 2 May 2020

DOI: 10.1002/jrs.5905

RESEARCH ARTICLE

Journal of RAMAN SPECTROSCOPY WILEY

Surface-enhanced resonance Raman scattering in partially oxidized thin copper film

Muhammad Farooq Saleem[1,3,4] | **Yasir Abdul Haleem**[2] | **Wenhong Sun**[3] | **Lei Ma**[4] | **Deliang Wang**[1]

[1]Hefei National Laboratory for Physical Sciences at the Microscale, University of Science and Technology of China, Hefei, China

[2]Department of physics, Khwaja Fareed University of Engineering and Information Technology, Rahim Yar Khan, Pakistan

[3]Research Center for Optoelectronic Materials and Devices, School of Physical Science and Technology, Guangxi University, Nanning, China

[4]Tianjin International Center for Nanoparticles and Nanosystems, Tianjin University, Tianjin, China

Correspondence
Deliang Wang, Hefei National Laboratory for Physical Sciences at the Microscale, University of Science and Technology of China, Hefei, 230026 Anhui, China.
Email: eedewang@ustc.edu.cn

Funding information
National Natural Science Foundation of China, Grant/Award Numbers: 61774140, 61474103, 11774255; Double First-Class initiative of Tianjin University from the Departement of Education of China and the Key Project of Natural Science Foundation of Tianjin City, Grant/Award Number: 17JCZDJC30100

Abstract

Broad and low-intensity Raman peaks are usually expected from nanocrystalline thin semiconductor films. The inherently weak Raman scattering phenomenon can be further deteriorated by unwanted background signals preventing the successful Raman analysis of an analyte. In this study, the resonant and surface-enhanced Raman scattering techniques were combined to detect CuO and Cu_2O phases in the partially oxidized nanocrystalline copper film that were otherwise undetectable. Heat treatment resulted in increased oxidation and phase transition from multiphase to single CuO phase that was in situ observed by temperature-dependent Raman measurements. Detailed understanding of the film properties and substrate interaction was made by using several characterization techniques.

KEYWORDS

copper oxide, phase transition, resonance, surface-enhanced Raman scattering

1 | INTRODUCTION

The oxides of transition metals such as cobalt, nickel, copper, iron, and zinc have many optical and electronic device applications particularly in storage media, gas sensing, lithium ion batteries, and solar cells.[1,2] Particularly, the oxides of naturally abundant copper have attracted much attention for their low cost and environment friendly semiconductors. They have aroused considerable interest due to their favorable electrical, optical, and magnetic properties.[3–6] They provide the basis for many high-temperature superconductors.[1,3,7] In order to achieve high device performances, it is crucial to deeply explore the electronic, optical, and vibrational properties of these oxides.

Correction added on 09 Jun 2020, after first online publication: the second, third and fourth authors were linked to the incorrect affiliations. The links have been corrected.

Thin oxide films of copper can be prepared both by chemical and physical routes including molecular beam epitaxy,[8] thermal oxidation,[9] evaporation,[2] electrochemical deposition,[10] spray pyrolysis,[11] and sputtering.[12] Thermal oxidation of copper in the air is the simplest and most economic method. As-deposited oxide films of copper are reported to have single and mixed crystal phases.[13–17] The relatively stable oxides of copper form cubic (I) (Cu_2O) and monoclinic tenorite (II) (CuO) phases with band gaps ranging between 1.2–2.2 eV.[13,15] CuO and Cu_2O are p-type semiconductors with indirect and direct band gaps, respectively. Exposure of freshly cleaned copper surface to air results in its immediate oxidation.[18] Thermal oxidation of Cu_2O and mixed-phase films results in the phase transition to CuO at high temperature.[9,19–23] The control on phase purity, crystal quality, and the extent of oxidation are essential for better device performance.

Glass slide is the most commonly used supporting substrate for Raman analysis of thin films. The glass substrate below few nanometers of a thin film is also in focus to the laser. The unwanted background Raman and fluorescence signals from the supporting substrate can deteriorate the desirable Raman signal of an analyte.[24] The poor Raman sensing in such cases is a consequence of the competition between Raman scattering in the analyte and unwanted background signals. Surface-enhanced Raman scattering (SERS) is a technique that employs metal nanoparticles and roughened metal surfaces to enhance an inherently poor Raman signal. The powerful resonant Raman scattering (RRS) and SERS techniques when combined can enhance the Raman signal of an analyte several fold.[16,25–28] Surface-enhanced resonance Raman scattering in a metal oxide sputtered on Ag film was first demonstrated by Thi.[29] In this study, we have combined the RRS and SERS techniques to successfully detect both the CuO and Cu_2O phases in the partially oxidized copper film ((Cu_xO); $1 \leq x \leq 2$) deposited on the silver nanoparticles (AgNPs) coated glass substrate (Cu_xO/AgNPs/glass). In addition, in situ temperature-dependent Raman spectroscopy has been employed to monitor the complete air oxidation dynamics of Cu_xO film.

2 | MATERIALS AND METHODS

A thin (~17 nm) silver film was evaporated on a clean glass substrate by thermal evaporation in vacuum. AgNPs were obtained by heating the silver film at 300°C for 45 min in nitrogen ambient. Partially oxidized thin (~20 nm) copper films were deposited both on a bare glass and a AgNPs/glass substrate by radio frequency (RF) sputtering at room temperature. During the film deposition, the ratio of oxygen to argon was adjusted to 1:2.

Raman spectra were obtained by using a LABRAM-HR micro-Raman system with 514.5- (Ar ion), 632.8-, and 785-nm laser light. Temperature-dependent Raman spectra were obtained by using the 514.5-nm laser. Raman spectroscope has a software-controlled temperature-regulating system that allows precise temperature control in the range of 25°C to 410°C. In order to reach the thermal equilibrium between the sample and the heating stage, the temperature was allowed to stabilize for 2 min before each Raman spectrum was recorded. Optical absorption measurements were carried out by using a SOLID3700 ultraviolet (UV)–visible spectrometer. Photoluminescence (PL) measurements were conducted by using the 532-nm laser of a LABRAM-HR micro-Raman system.

The X-ray photoelectron spectroscopy (XPS) was performed using an ESCALAB 250 spectrometer. The film morphology and structure were investigated by using a SIRION200 scanning electron microscopy (SEM) and a Rigaku TTR III X-ray diffractometer (XRD) with Cu Kα radiation source (λ of 0.154 nm).

3 | RESULTS AND DISCUSSION

AgNPs with an average ~50 nm size were employed to achieve SERS in Cu_xO film. The surface morphology and UV–visible absorption properties of AgNPs fabricated on glass have been reported elsewhere.[27] The change in color of the AgNPs/glass occurred after the deposition of copper film, in agreement with our previous report.

In this study, the surface-enhanced and RRS techniques were combined to detect the two distinct phases of copper oxide in the partially oxidized copper film by depositing it on AgNPs/glass and by tuning the laser wavelengths to achieve resonance. The complete air oxidation dynamics of the partially oxidized film were monitored by in situ temperature-dependent SERS from room temperature up to 410°C. PL spectroscopy was performed to quantify the fluorescence contribution of the substrate to the Raman signal of the Cu_xO film. As-deposited film was also investigated by XPS to probe the copper oxidation states and identify the crystal phases. The variations in film structure and grain size upon heat treatment were investigated by SEM and XRD. UV–visible spectroscopy was used to explore the optical properties of the as-deposited and heat-treated film.

3.1 | SEM measurements

Figure S1 shows the SEM surface images of the as-deposited and the heat-treated Cu_xO film. The as-

deposited film exhibits continuous and homogenous flake-like morphology (Figure S1a), which turns into nanoscale granular structures after heat treatment at 170°C as shown in Figure S1b. With further heating at 320°C and 410°C, the small particles merged and formed micro-scale particles as shown in Figure S1c and d, respectively. The surface morphology changed a lot after heating, which can be attributed to increased thermal oxidation and the variation in grain size.

3.2 | XRD measurements

The crystalline structure of the as-grown and the heat-treated copper film was characterized by XRD as shown in Figure S2. In order to get high signal-to-noise ratio from XRD, a copper film of ~100-nm thickness was prepared by RF sputtering. The diffraction patterns show three reflections at 2θ values of 33.26°, 35.60°, and 39.50° for the as-deposited and the heat-treated copper oxide film as shown in Figure S2. All these peaks are indexed as crystallographic reflections of (110), (−111), and (111) planes of monoclinic CuO.[30] The grain size of the film, estimated by the full width at half maximum (FWHM), shrinks from 16 to 10 nm after heat treatment.[19,31] It can be concluded that the large particles formed at high temperature (Figure S1c and d) are made of nanoscale grains. It should be noted that XRD was unable to detect the minor Cu_2O phase that was present in the as-deposited film as confirmed by the Raman spectroscopy and the XPS data mainly due to its inherently poor sensitivity to minor phases.[21,27,32] The powerful combination of RRS and SERS techniques enabled the detection of both the major CuO and minor Cu_2O phases in the film as will be discussed in the following. Moreover, the pure copper that was present as a minor phase in the film was also not detected by XRD.

3.3 | XPS measurements

High-resolution XPS was used to further confirm the material composition as shown in Figure 1. In Figure 1a, the peaks at 934.9 and 954.7 eV are the core-level binding energies of $Cu2p_{3/2}$ and $Cu2p_{1/2}$, respectively. The binding energy difference of ~19.8 eV between the $Cu2p_{1/2}$ and $Cu2p_{3/2}$ peaks is in close agreement with the reported energy difference for CuO.[21] The characteristics shake-up satellite structures of CuO at binding energies 9.1 and 7.6 eV higher than $Cu2p_{3/2}$ further confirm the formation of CuO phase.[33,34] The binding energy peaks do not have a single symmetric shape. The asymmetric broadening is mainly due to the presence of three different phases in the amorphous film including CuO, Cu_2O, and pure metal.[35] The fitting of the main $Cu2p_{3/2}$ peak gives three peaks at energy values of 934.8, 933.0, and 932.1 eV, which correspond to CuO, Cu_2O, and Cu phases respectively, as shown in Figure 1b.[3,19,20,36] The fitting of O1s peak gives two peaks representing the distinct chemical states of oxygen as shown in Figure 1c. The main broad peak at 531.8 eV is attributed to the oxygen in Cu-O bond.[37,38] The peak fitted at 530.1 eV is associated with oxygen in Cu_2O.[11,39–41] The peak at 533.1 eV indicates the presence of hydroxyl groups, which might arise due to the exposure of oxide film to the open air.[36,42] As the film is predominantly made of CuO phase, successful detection of this phase with most of the characterization techniques is quite obvious.

3.4 | UV–visible absorption spectroscopy measurements

For a more reliable Raman analysis of an analyte, many competing mechanisms need to be addressed including unwanted Raman signals of the substrate and fluorescence background interferences that can deteriorate an inherently weak Raman signal. Raman enhancement

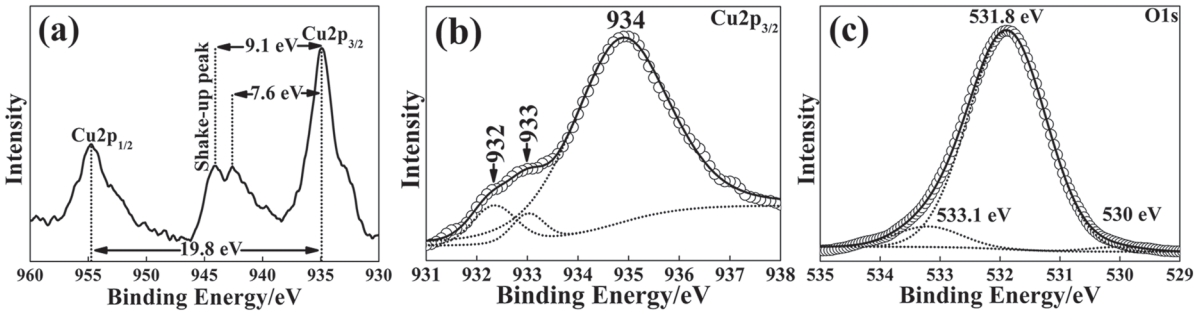

FIGURE 1 X-ray photoelectron spectroscopy (a) Cu2p core-level spectrum, (b) fitted $Cu2p_{3/2}$ spectrum, and (c) fitted O1s spectrum for as-deposited Cu_xO/glass sample

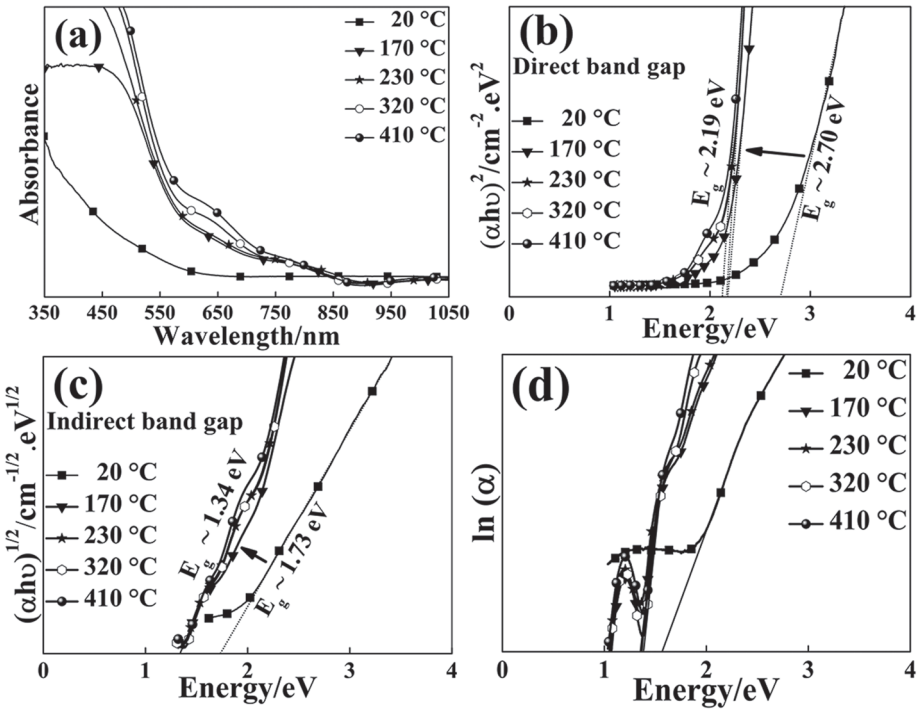

FIGURE 2 (a) The ultraviolet–visible absorption spectra of the as-deposited and heat-treated thin films at different temperatures. Energy band gaps measured by assuming the material to be (b) direct and (c) indirect band gap. (d) Plot of $ln(\alpha)$ versus energy to determine Urbach energy values

over unwanted background signals can be achieved by combining the powerful RRS and SERS techniques. SERS can be achieved by depositing an analyte on plasmonic metal nanoparticles or on roughened metal surfaces. In such a system, surface-enhanced resonance Raman scattering can be achieved by tuning the Raman laser to an energy value higher than or close to that of an electronic transition in the analyte that can also be a transition in the band gap of the material.[27,43]

To investigate the optical absorption properties of the as-deposited and heat-treated film, the UV–visible absorption spectra were measured in the wavelength range of 350–1,050 nm, as shown in Figure 2a. The band gap values were calculated by using Tauc plot that are based on the equation $\alpha = C\ (h\nu - E_g)^n$, where α is the coefficient of optical absorption, C is a constant, $h\nu$ is the photon energy, E_g is the energy band gap of the material under investigation, and n is a number that can have a value of either 1/2 or 2 depending on whether the material is a direct or or an indirect band gap material, respectively. The linear extrapolation of the plot of $(\alpha h\nu)^n$ versus $h\nu$ down to the photon energy axis gives the E_g values as shown in Figure 2b,c. As the XPS data suggest that the film contains Cu_2O (direct band gap) and CuO (indirect band gap) crystal phases, it is not easy to speculate whether the resulting film has a direct or indirect band gap. As will be discussed in the following, the high-intensity Raman bands associated with Cu_2O compared with CuO phase indicate that Cu_2O is the dominant phase as the intensity of Raman scattering is directly proportional to the number of scattering centers present in the volume illuminated.[19] However, the XRD data that usually give more reliable information about the dominant phases suggest that the dominant phase is CuO. Therefore, both the direct and indirect band gaps were calculated. For as-deposited film, the E_g values of 2.7 and 1.7 eV were obtained for direct and indirect band gaps, respectively. The band gap values of the as-deposited film are higher than those reported for CuO and Cu_2O due to quantum size effect.[44] In the absorption spectra, it can be seen that the as-deposited film has low absorption rate compared with that of the annealed film and that the absorbance increases after heat treatment, indicating band gap shrinkage. The absorption spectrum of the as-deposited film is similar to that reported for pure metallic copper.[45] It can be deduced that the highly transparent films can be obtained from pure and mixed-phase partially oxidized copper films.

The direct band gap decreased to 2.19 eV, whereas the indirect band gap decreased to 1.36 eV after heat treatment due to increased oxidation and change in film structure as shown in Figure 2b,c. The absorption and band gap of the Cu_xO film changed rapidly after heat treatment until 320°C, which confirms that the as-deposited film was partially oxidized and that heat treatment increased the oxidation of the film, leading to values close to that of reported for copper oxides.[13,15] As was confirmed by the temperature-dependent Raman spectra, the mixed-phase Cu_xO film had undergone phase transition to CuO above 320°C

and the band gap did not change much above this temperature for the single-phase film.

Room temperature deposited film can have a large number of defects and disorder. Increased defects result in increased localized disorder states that extend in the band gap of the material introducing intragap states.[46] Urbach energy or Urbach tail (E_u) is an important parameter that can be used to quantify the disorder in a thin film. A graph between $ln(\alpha)$ versus energy is used to calculate E_u. The inverse of the slope of the straight line in the graph gives E_u values as shown in Figure 2d. The E_u values decreased from 0.37 to 0.17 eV after heating. Higher E_u value for as-deposited film indicates that the defect levels exist below the conduction band edge due to incomplete oxidation, multiphase structures, and poor crystallinity.[47] Decreasing trend in E_u values after heating is due to increased oxidation, improvement in crystal quality, and increased long range order.[48,49] The E_u values for the heat-treated film are not very high compared to the values reported for CuO and Cu_2O, indicating better crystal quality.[5,50–52]

3.5 | Raman spectroscopy and PL measurements

Tuning of the Raman laser wavelength is a possible way to achieve RRS in a Raman-active material. To explore the resonance conditions, the Cu_xO/glass and Cu_xO/AgNPs/glass were characterized with three different Raman laser light of 514.5, 632.8, and 785.0 nm wavelengths at room temperature as shown in Figure 3a, b.

The Raman spectra obtained were compared with the spectra of bare glass substrate as shown in Figure 3c. The glass is known to emit fluorescence spectrum with 785-nm laser.[53] The Raman spectra for Cu_xO/glass, Cu_xO/AgNPs/glass and bare glass samples look similar when excited by 785-nm laser. It can be seen that no characteristic Raman signatures of Cu_xO were observed with this wavelength.

The Raman spectra for the Cu_xO/glass and the Cu_xO/AgNPs obtained by 514.5-nm laser resemble that of the bare glass substrate as shown in Figure 3a–c. The Raman peak of glass located in the wavenumber range of 400–600 cm^{-1} becomes symmetric upon copper film deposition. It can be deduced that the Raman spectrum of Cu_xO is buried under the strong glass background and fluorescence signals when excited by 514.5-nm laser. The glass peak disappears when the Cu_xO/AgNPs/glass is excited by 632.8-nm laser and the low-intensity Raman modes of Cu_xO show up as shown in Figure 3b. The spectrum for the Cu_xO/AgNPs/glass sample taken by 632.8-nm laser shows the A_g, B_{1g}, and B_{2g} modes of CuO at 280, 332, and 603 cm^{-1} respectively.[54,55] A peak at 470 cm^{-1} is also assigned to CuO.[55] The peaks at 112, 154, 235, 408, and 525 cm^{-1} are assigned to Cu_2O phase.[55–57] Observation of so many modes in one spectrum is surely a consequence of powerful combination of RRS and SERS. The width of the A_g mode of major CuO phase is 26 cm^{-1}. The broad peaks are usually considered

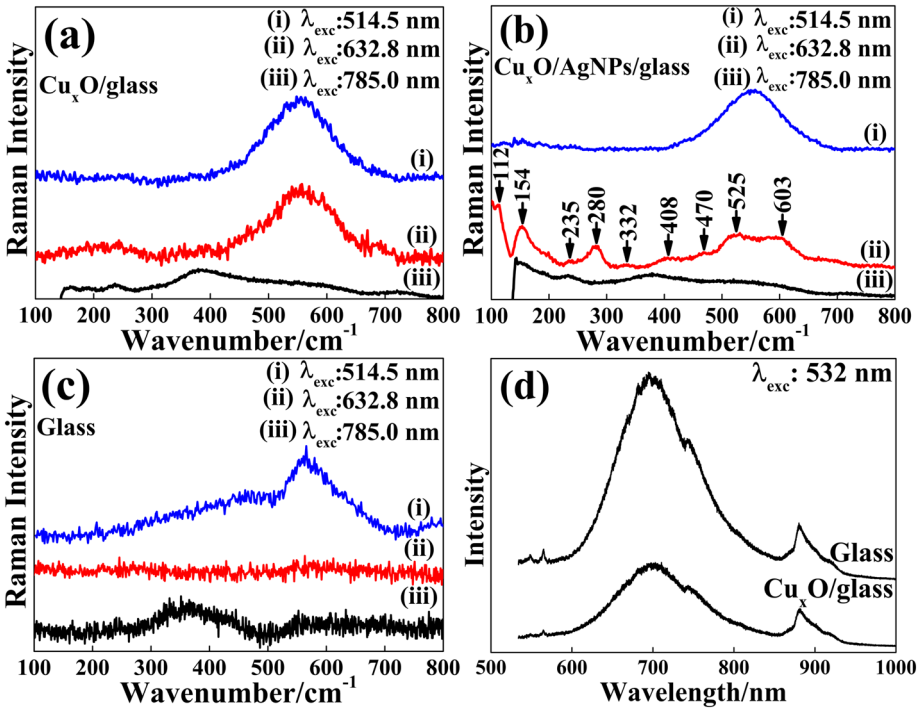

FIGURE 3 Raman spectra of (a) Cu_xO/glass, (b) Cu_xO/AgNPs/glass, and (c) glass. (d) Photoluminescence spectra of glass and Cu_xO/glass obtained by 532-nm laser

to arise from defects, poor crystallinity, and size effect.[7,36,58,59] As indicated by the XRD data, the broad Raman peaks in our work are mainly due to size effect and vibrational confinement in radial direction for nanocrystalline film. The poor crystallization and defects due to oxygen deficiency in the room temperature deposited Cu_xO film might also have contributed to the increased width.[7,59] It should be noted that XRD could not detect the minor Cu_2O and Cu phases owing to its inherently poor sensitivity to minor phases. The wavelength tunability and SERS make Raman spectroscopy a powerful technique when it comes to detection of minor phases, which is not possible with XRD. It can be concluded that 632.8-nm laser is in close resonance to the film and that the effective band gap of the multiphase Cu_xO film is somewhere near to the energy of this laser ($E \sim 1.95$ eV). SERS results in the formation of a charge transfer complex between AgNPs and Cu_xO that defines the conditions for resonance enhancement with a particular Raman excitation laser. The strong surface plasmon resonance absorption of the plasmonic AgNPs quenched the fluorescence background.[60] The overall poor sensitivity of most of the lasers towards Cu_xO is due to strong glass background and inherently poor Raman scattering in nanocrystalline film.[7,57]

No glass peaks were observed when the 632.8-nm laser was used on the bare glass, as shown in Figure 3c. However, glass peak appeared upon Cu_xO deposition as shown in Figure 3a. It can be deduced that the partially oxidized metallic film caused SERS in the glass that dominated the weak Cu_xO signal. Due to its relatively poor penetration to the thin nanocrystalline film of higher surface-to-volume ratio, the 632.8-nm laser limits its penetration to copper film and the underlying glass substrate goes out of focus to the laser, resulting in weak glass features.[7] A clear trade-off between the Raman signal of Cu_xO and unwanted background signals occurs, and the Raman signal of Cu_xO dominates. Strong plasmonic resonance coupling phenomenon occurs due to the combined power of SERS and RRS, which results in measurable Raman signal. It can be noticed that the Raman spectra for the Cu_xO/AgNPs/glass have high signal-to-noise ratio compared with those of the Cu_xO/glass, which is certainly a consequence of SERS.

To quantify the influence of glass fluoresce signal on Raman spectra, the PL spectra of glass and Cu_xO/glass samples were obtained by using 532-nm laser as shown in Figure 3d. It can be observed that the glass florescence signal dominates for the both samples and no PL emission peaks of Cu_xO were observed, leading to poor Raman scattering in Cu_xO with 514.5-nm Raman laser.

Heat treatment of the copper in air leads to increased oxidation. To investigate the oxidation dynamics of as-deposited Cu_xO film, the temperature-dependent Raman spectra for the Cu_xO/AgNPs/glass samples were in situ recorded from room temperature to 410°C using 514.5-nm excitation laser, as shown in Figure 4a. Few of the important Raman spectra are shown separately in Figure 4b for clarity. The broad substrate signal dominates until 140°C due to the off resonance of the partially oxidized film with 514.5-nm wavelength. The A_g and B_{1g} modes of CuO appeared above 170°C as very low-intensity broad modes in the wavenumber range of 250–450 cm^{-1}, which red shifted with the increase in temperature due to lattice expansion.[38,56] Two peaks at 154 and 218 cm^{-1} also appeared below 170°C that are assigned to Cu_2O phase. The 154 cm^{-1} Raman mode showed significant red shift with temperature. A peak at 218 cm^{-1} is common in Cu_2O and AgO[61–63]; however, its simultaneous appearance with 154 cm^{-1} mode of Cu_2O confirms that it is from Cu_2O. The Cu_2O formation temperature is also in agreement with literature.[9,19–22] A Raman mode near 220 cm^{-1} is known as two-phonon scattering of a mode at around 110 cm^{-1}.[21] The position of this peak almost remained constant. The intensities of 154 and 218 cm^{-1} peaks first increased and then decreased at high temperature. The Raman signals of CuO, Cu_2O, and glass result in complicated Raman

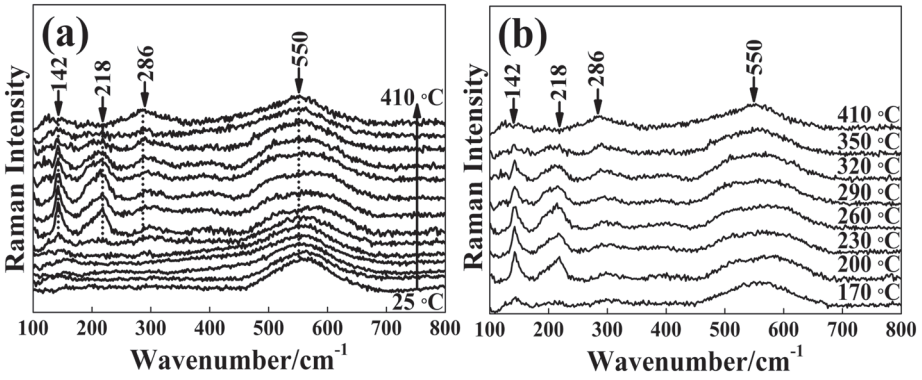

FIGURE 4 (a) Temperature-dependent Raman spectra of Cu_xO/AgNPs/glass. (b) A few distinct Raman spectra redrawn together to show detailed features of the peaks

spectrum. The coexistence of CuO and Cu_2O has been reported previously.[19,20,22] From the temperature-dependent Raman data in the range 170–320°C, one might assume that the dominant phase in this temperature range is Cu_2O due to higher intensity of the associated Raman peaks compared with CuO. However, XRD data confirm that the major phase is CuO. The absence of Cu_2O-related peaks in XRD patterns of the as-deposited and the heat-treated film is due to the low sensitivity of XRD to minor phases compared with Raman spectroscopy.[19,21] The increased Raman sensitivity to Cu_2O compared with CuO can be associated with the breakdown of selection rules due to resonance in fundamental electronic transition in the crystal.[44] The band gap and resonance conditions also change with heating in agreement with UV–visible absorption data. The overall increased Raman sensitivity upon heating is associated with transition of the film from partially metallic to semiconducting.

The shape of the broad glass mode changes above 170°C attributed to the contribution from 408, 470, 525, and 603 cm^{-1} modes of Cu_xO in agreement with room temperature data obtained by 632.8-nm laser. The high temperature stability of glass suggests that most of the vibrational changes due to temperature should occur in phonon modes of the film. The heat treatment until 260°C caused further oxidation of the film and improvement of the crystallinity of Cu_2O phase, resulting in intense and sharp peaks related to this phase. The peaks were broadened and red shifted upon heating above 260°C, as shown in Figure 4. The broad peaks are usually considered to arise from defects, poor crystallinity, and size effect,[7,36,58,59] but the relatively small Urbach energy value of the heat-treated film suggests that the quality of the film is reasonably good.[50–52,55] It can be concluded that the broad and low-intensity peaks in our work arise from grain size reduction of nanocrystalline film as indicated by XRD.[7,58,59] The increased surface-to-volume ratio limits the penetration of Raman laser light into the sample resulting in broad and red-shifted peaks.

The intensity of Cu_2O-related modes decreases above 260°C due to phase transition from Cu_2O to CuO until 350°C. The Cu_2O-related modes disappear above this temperature and a broad red-shifted A_g mode of CuO is observed, attributed to phase transition from mixed-phase to pure CuO. The A_g mode shows asymmetric broadening towards lower wavenumber side due to the contribution of low-intensity B_{1g} mode of CuO. The phonon softening occurs as a consequence of thermal expansion and increased phonon vibrational amplitude at high temperature.[2,7] It should be noted that a low-intensity peak near 300 cm^{-1} also appears in theRaman spectra above 170°C that red shifts with temperature. The sharpening of this peak and the weakening of Cu_2O-related modes at high temperatures confirm the phase transition of Cu_2O to CuO with temperature. A small hump near 400 cm^{-1} (originally at 412 cm^{-1}) is also observable above 200°C, which can be associated with fourth-order overtone of Cu_2O.[55–57] The hump remains observable until all the Cu_2O transforms to CuO. Phase transition from Cu_2O to CuO at high temperature is in agreement with previous studies.[10,20–24] The calculated indirect band gap value for the film heated at 410°C is also in agreement with that of reported values for CuO. CuO normally shows a broad B_{2g} mode in the 500–650 cm^{-1} region.[22] The glass mode broadens at high temperature due to lattice expansion and contribution from broad CuO-related mode in this wavenumber region.

Unlike XRD, Raman spectroscopy successfully detected the minor Cu_2O phase due to increased nanoplasmonic electric field of AgNPs. It can be concluded that the Raman features of as-deposited Cu_xO were masked by the unwanted background. After heating, the optical absorption was increased due to band gap shrinking and the Cu_xO peaks overwhelmed those of substrate. However, the Raman intensity is yet very low due to nanocrystalline nature of the film, which further deteriorates at high temperature due to increased thermal expansion.[2,7,23,36,58,64] In such cases, surface-enhanced resonance Raman scattering proves to be the most sensitive material characterization technique.

4 | CONCLUSION

The powerful surface-enhanced and resonance Raman scattering techniques were successfully combined to make the inherently weak Raman signals of multiphase copper oxide film measurable. It allowed the measurement of a Raman spectrum with clearly distinguishable peaks from both the CuO and Cu_2O phases present in the film. The inherently weak Raman scattering in the film was attributed to the strong Raman and fluorescence background interferences of underlying glass substrate and nanocrsytalline nature of the film. The high-intensity Raman peaks of minor Cu_2O phase compared with those of CuO were explained in terms of breakdown of selection rules and the different resonance conditions for different material phases present in the multiphase film. Heating resulted in increased oxidation, band gap reduction, and phase transition of the film from mixed to pure CuO phase.

ACKNOWLEDGEMENTS

Financial support is acknowledged from the National Natural Science Foundation of China (61774140, 61474103 and 11774255), Double First-Class initiative of Tianjin University from the Departement of Education of

China and the Key Project of Natural Science Foundation of Tianjin City (17JCZDJC30100).

ORCID

Muhammad Farooq Saleem https://orcid.org/0000-0001-6133-0810
Deliang Wang https://orcid.org/0000-0002-3274-9249

REFERENCES

[1] L. Debbichi, M. C. Marco de Lucas, J. F. Pierson, P. Kruger, *J. Phys. Chem. C* **2012**, *116*, 10232.
[2] S. Ravi, A. B. Kaiser, C. W. Bumby, *J. Appl. Phys. (Melville, NY, U. S.).* **2015**, *118*, 085311.
[3] D. Tahir, S. Tougaard, *J. Phys. Condens. Matter* **2012**, *24*, 175002.
[4] N. R. Dhineshbabu, V. Rajendran, N. Nithyavathy, R. Vetumperumal, *Appl. Nanosci.* **2016**, *6*, 933.
[5] D. Manikandan, S. Mohan, P. Magudapathy, K. G. M. Nair, *Physica B Condens. Matter.* **2003**, *325*, 86.
[6] D. Manikandan, S. Mohan, K. G. M. Nair, *Mater. Lett.* **2003**, *57*, 1391.
[7] J. F. Xu, W. Ji, Z. X. Shen, W. S. Li, S. H. Tang, X. R. Ye, D. Z. Jia, X. Q. Xin, *J. Raman Spectrosc.* **1999**, *30*, 413.
[8] K. P. Muthe, J. C. Vyas, N. N. Savita, D. K. Aswal, S. K. Gupta, D. Bhattacharya, R. Pinto, G. P. Kothiyal, S. C. Sabharwal, *Thin Solid Films* **1998**, *324*, 37.
[9] L. de Los Santos Valladares, D. H. Salinas, A. B. Dominguez, D. A. Najarro, S. I. Khondaker, T. Mitrelias, C. H. W. Barnes, J. A. Aguiar, Y. Majima, *Thin Solid Films* **2012**, *520*, 6368.
[10] A. Roy, S. J. Harsharaj, M. Cho, J. G. Seo, *J. Ind. Eng. Chem. (Amsterdam, Neth.).* **2019**, *76*, 515.
[11] J. Morales, L. Sanchez, F. Martin, J. R. Ramos-Barrado, M. Sanchez, *Thin Solid Films* **2005**, *474*, 133.
[12] C. Shinho, *Met. Mater. Int.* **2013**, *19*, 1327.
[13] T. Maruyama, *Sol. Energy Mater. Sol. Cells* **1998**, *56*, 85.
[14] X. P. Gao, J. L. Bao, G. L. Pan, H. Y. Zhu, P. X. Huang, F. Wu, D. Y. Song, *J. Phys. Chem. B* **2004**, *108*, 5547.
[15] M. R. Johan, M. S. Mohd Suan, N. L. Hawari, H. Y. Ching, *Int. J. Electrochem. Sci.* **2011**, *6*, 6094.
[16] O. Prakash, S. Kumar, P. Singh, V. Deckert, S. Chatterjee, A. K. Ghosh, R. K. Singh, *J. Raman Spectrosc.* **2016**, *47*, 813.
[17] K. H. Yoon, W. J. Choi, D. H. Kang, *Thin Solid Films* **2000**, *372*, 250.
[18] S. K. Chawla, B. I. Rickett, N. Sankarraman, J. H. Payer, *Corros. Sci.* **1992**, *33*, 1617.
[19] Y. S. Gong, C. Lee, C. K. Yang, *J. Appl. Phys. (Melville, NY, U. S.).* **1995**, *77*, 5422.
[20] B. Balamurugan, B. R. Mehta, D. K. Avasthi, F. Singh, A. K. Arora, M. Rajalakshmi, G. Raghavan, A. K. Tyagi, S. M. Shivaprasad, *J. Appl. Phys. (Melville, NY, U. S.)* **2002**, *92*, 3304.
[21] Z. H. Gan, G. Q. Yu, B. K. Tay, C. M. Tan, Z. W. Zhao, Y. Q. Fu, *J. Phys. D Appl. Phys.* **2003**, *37*, 81.
[22] L.-C. Chen, C.-C. Chen, K.-C. Liang, S. H. Chang, Z.-L. Tseng, S.-C. Yeh, C.-T. Chen, W.-T. Wu, C.-G. Wu, *Nanoscale Res. Lett.* **2016**, *11*, 402.
[23] L. George, A. Gupta, P. R. Shaina, N. D. Gupta, M. Jaiswal, *Nanotechnology* **2015**, *26*, 495701.
[24] D. Tuschel, **2016**
[25] G. Satpathy, G. K. Chandra, E. Manikandan, D. R. Mahapatra, S. Umapathy, *Biotechnol. Lett.* **2020**, *42*, 853.
[26] P. Manikandan, D. Manikandan, E. Manikandan, A. C. Ferdinand, *Spectrochim. Acta A Mol. Biomol. Spectrosc.* **2014**, *124*, 203.
[27] M. F. Saleem, H. Zhang, Y. Deng, D. Wang, *J. Raman Spectrosc.* **2017**, *48*, 224.
[28] P. Manikandan, D. Manikandan, E. Manikandan, A. C. Ferdinand, *Plasmonics.* **2014**, *9*, 637.
[29] M. P. Thi, *Chem. Phys. Lett.* **1985**, *115*, 130.
[30] A. Sharma, M. Varshney, J. Park, T.-K. Ha, K.-H. Chae, H.-J. Shin, *RSC Adv.* **2015**, *5*, 21762.
[31] J. F. Pierson, A. Thobor-Keck, A. Billard, *Appl. Surf. Sci.* **2003**, *210*, 359.
[32] B. P. Dhonge, S. S. Ray, B. Mwakikunga, *RSC Adv.* **2017**, *7*, 21703.
[33] L. Debbichi, M. C. M. de Lucas, P. Krüger, *Mater. Chem. Phys.* **2014**, *148*, 293.
[34] Z.-S. Hong, Y. Cao, J.-f. Deng, *Mater. Lett.* **2002**, *52*, 34.
[35] M. C. Biesinger, *Surf. Interface Anal.* **2017**, *49*, 1325.
[36] J. Han, X. Zong, X. Zhou, C. Li, *RSC Adv.* **2015**, *5*, 10790.
[37] R. Shabu, A. M. E. Raj, C. Sanjeeviraja, C. Ravidhas, *Mater. Res. Bull.* **2015**, *68*, 1.
[38] V. Senthilkumar, Y. S. Kim, S. Chandrasekaran, B. Rajagopalan, E. J. Kim, J. S. Chung, *RSC Adv.* **2015**, *5*, 20545.
[39] C. Zhu, A. Osherov, M. J. Panzer, *Electrochim. Acta* **2013**, *111*, 771.
[40] M. Okada, L. Vattuone, K. Moritani, L. Savio, Y. Teraoka, T. Kasai, M. Rocca, *Phys. Rev. B* **2007**, *75*, 233413.
[41] J. Ghijsen, L.-H. Tjeng, J. V. Elp, H. Eskes, J. Westerink, G. A. Sawatzky, M. T. Czyzyk, *Phys. Rev. B* **1988**, *38*, 11322.
[42] E. Cano, J. M. Bastidas, J. L. Polo, N. Mora, *J. Electrochem. Soc.* **2001**, *148*, 431.
[43] N. A. M. Shanid, M. A. Khadar, V. G. Sathe, *J. Raman Spectrosc.* **2011**, *42*, 1769.
[44] H. Wang, J. Xu, J. Zhu, H. Chen, *J. Cryst. Growth* **2002**, *244*, 88.
[45] P. Christian, M. Bromfield, *J. Mater. Chem.* **2010**, *20*, 1135.
[46] I. Kashif, A. Ratep, *J. Mol. Struct.* **2015**, *1102*, 1.
[47] A. Somvanshi, S. Husain, W. Khan, *J. Alloys Compd.* **2019**, *778*, 439.
[48] M. Ledinsky, T. Schönfeldová, J. Holovský, E. Aydin, Z. Hájková, L. Landová, N. Neyková, A. Fejfar, S. D. Wolf, *J. Phys. Chem. Lett.* **2019**, *10*, 1368.
[49] F. Ye, J. J. Zeng, X. M. Cai, X.-Q. Su, B. Wang, H. Wang, V. A. L. Roy, *J. Alloys Compd.* **2017**, *721*, 64.
[50] I. Y. Bouderbala, A. Herbadji, L. Mentar, A. Beniaiche, A. Azizi, *J. Electron. Mater.* **2018**, *47*, 2000.
[51] Y. Wang, P. Miska, D. Pilloud, D. Horwat, F. Mücklich, J.-F. Pierson, *J. Appl. Phys. (Melville, NY, U. S.)* **2014**, *115*, 073505.
[52] P. K. Singh, A. K. Das, G. Hatui, G. C. Nayak, *Mater. Chem. Phys.* **2017**, *198*, 16.

[53] C. Raml, X. He, M. Han, D. R. Alexander, Y. Lu, *Opt. Lett.* **2011**, *36*, 1287.
[54] Y. Deng, A. D. Handoko, Y. Du, S. Xi, B. S. Yeo, *ACS Catal.* **2016**, *6*, 2473.
[55] H. Y. H. Chan, C. G. Takoudis, M. J. Weaver, *J. Phys. Chem. B* **1999**, *103*, 357.
[56] L. Yang, J. Lv, Y. Sui, W. Fu, X. Zhou, J. Ma, S. Su, W. Zhang, P. Lv, D. Wu, Y. Mua, H. Yang, *CrstEngComm* **2014**, *16*, 2298.
[57] H. Zhang, D. Zhang, L. Guo, R. Zhang, P. Yin, R. Wang, *J. Nanosci. Nanotechnol.* **2008**, *8*, 6332.
[58] P. H. Shih, C. L. Cheng, S. Y. Wu, *Nanoscale Res. Lett.* **2013**, *8*, 1.
[59] F. A. Akgul, G. Akgul, N. Yildirim, H. E. Unalan, R. Turan, *Mater. Chem. Phys.* **2014**, *14*, 987.
[60] A. K. Pal, D. B. Mohan, *Mater. Res. Express.* **2014**, *1*, 025014.
[61] G. I. N. Waterhouse, G. A. Bowmaker, J. B. Metson, *Phys. Chem. Chem. Phys.* **2001**, *17*, 3838.
[62] P. Colomban, A. Tournié, M. Maucuer, P. Meynard, *J. Raman Spectrosc.* **2012**, *43*, 799.
[63] M. R. Joya, J. Barba-Ortega, A. M. Raba, *Indian J. Pure Appl. Phy.* **2019**, *57*, 268.
[64] T. H. Tran, V. T. Nguyen, *Mater. Sci. Semicond. Process.* **2016**, *46*, 6.

SUPPORTING INFORMATION

Additional supporting information may be found online in the Supporting Information section at the end of this article.

How to cite this article: Saleem MF, Haleem YA, Sun W, Ma L, Wang D. Surface-enhanced resonance Raman scattering in partially oxidized thin copper film. *J Raman Spectrosc*. 2020;1–9. https://doi.org/10.1002/jrs.5905